# $K^0 \leftrightarrow \overline{K}^0$ transitions monitored by strong interactions : a new determination of the $K\_L - K\_S$ mass difference

A. Angelopoulos, E. Aslanides, G. Backenstoss, P. Bargassa, O. Behnke, A. Benelli, V. Bertin, F. Blanc, P. Bloch, P. Carlson, et al.

# $K^0 \rightleftharpoons \overline{K}^0$ transitions monitored by strong interactions: a new determination of the $K_L - K_S$ mass difference

*CPLEAR Collaboration*

A. Angelopoulos[1], E. Aslanides[11], G. Backenstoss[2], P. Bargassa[13], O. Behnke[17], A. Benelli[2],
V. Bertin[11], F. Blanc[7,13], P. Bloch[4], P. Carlson[15], M. Carroll[9], E. Cawley[9], M.B. Chertok[3],
M. Danielsson[15], M. Dejardin[14], J. Derre[14], A. Ealet[11], C. Eleftheriadis[16], W. Fetscher[17],
M. Fidecaro[4], A. Filipčič[10], D. Francis[3], J. Fry[9], E. Gabathuler[9], R. Gamet[9], H.-J. Gerber[17],
A. Go[4], A. Haselden[9], P.J. Hayman[9], F. Henry-Couannier[11], R.W. Hollander[6], K. Jon-And[15],
P.-R. Kettle[13], P. Kokkas[8], R. Kreuger[6], R. Le Gac[11], F. Leimgruber[2], I. Mandić[10], N. Manthos[8],
G. Marel[14], M. Mikuž[10], J. Miller[3], F. Montanet[11], A. Muller[14] T. Nakada[13], B. Pagels[17],
I. Papadopoulos[16], P. Pavlopoulos[2], G. Polivka[2], R. Rickenbach[2], B.L. Roberts[3], T. Ruf[4],
L. Sakeliou[1], M. Schäfer[17], L.A. Schaller[7], T. Schietinger[2], A. Schopper[4], L. Tauscher[2],
C. Thibault[12], F. Touchard[11], C. Touramanis[9], C.W.E. Van Eijk[6], S. Vlachos[2], P. Weber[17],
O. Wigger[13], M. Wolter[17], D. Zavrtanik[10], D. Zimmerman[3]

**Abstract**

The CPLEAR set-up (modified) has been used to determine the $K_L$-$K_S$ mass difference by a method where neutral-kaon strangeness oscillations are monitored through kaon strong interactions, rather than semileptonic decays, thus requiring no assumptions on CPT invariance for the decay amplitudes. The result, $\Delta m = (0.5343 \pm 0.0063_{\text{stat}} \pm 0.0025_{\text{syst}}) \times 10^{10} \hbar/\text{s}$, provides a valuable input for CPT tests.

*(Submitted to Phys. Lett. B)*

[1] University of Athens, Greece
[2] University of Basle, Switzerland
[3] Boston University, USA
[4] CERN, Geneva, Switzerland
[5] LIP and University of Coimbra, Portugal
[6] Delft University of Technology, Netherlands
[7] University of Fribourg, Switzerland
[8] University of Ioannina, Greece
[9] University of Liverpool, UK
[10] J. Stefan Inst. and Phys. Dep., University of Ljubljana, Slovenia
[11] CPPM, IN2P3-CNRS et Université d'Aix-Marseille II, France
[12] CSNSM, IN2P3-CNRS, Orsay, France
[13] Paul Scherrer Institut (PSI), Switzerland
[14] CEA, DSM/DAPNIA, CE-Saclay, France
[15] Royal Institute of Technology, Stockholm, Sweden
[16] University of Thessaloniki, Greece
[17] ETH-IPP Zürich, Switzerland

# 1 Introduction

Very early, after the hypothesis of particle mixture had been advanced for $K^0$ and $\overline{K}^0$ [1], the change of strangeness content with time was predicted, as a consequence, for beams starting as pure $K^0$ or $\overline{K}^0$ [2]. Proposals followed how to monitor the strangeness oscillations and measure the $K_L$-$K_S$ mass difference $\Delta m$, that is the oscillation frequency modulus $\hbar$. It was suggested that starting with a pure $K^0$ (or $\overline{K}^0$) beam, one could observe the building up of a $\overline{K}^0$ (or $K^0$) flux by measuring either weak decays to $e\pi\nu$ [3] or the products of strong interactions in a thin slab of material [4, 5]. These suggestions were soon followed by the first experiments [4,6,7]. In another approach [8–10] it was shown that the intensity of the $K_S$ component transmitted through an absorber is a very sensitive function of the mean life $\tau_S$ and of the $K_L$-$K_S$ mass difference, and this led to the first of many variants of the regenerator method [11]. Later, this method provided results in the current range of accuracy [12–15] and even allowed the $\Delta m$ sign to be determined [16, 17]. Comparable accuracy was obtained with the oscillation method coupled to the measurement of semileptonic decays in Ref. [18], and recently by CPLEAR [19].

CPLEAR has revisited the oscillation method, tagging the strangeness of the neutral kaon by strong interaction at two different times. This work is reported in the present paper.

# 2 Principle of the measurement

The principle of the measurement consists in measuring the probability that a neutral kaon, created at $t = 0$ in a strangeness ($S = 1$ or $S = -1$) eigenstate, is found after a time $t = \tau$ in the same or opposite strangeness state. Each probability contains a $K_L$-$K_S$ interference term which is sensitive to $\Delta m$; moreover it is dependent on $\varepsilon$ and $\delta$, the T- and CPT-violation parameters of the neutral-kaon mixing matrix, thus

$$
\begin{aligned}
\mathcal{P}_+ &= \mathcal{P}(K^0{}_{t=0} \to K^0{}_{t=\tau}) \\
&= \frac{1}{4}[(1 + 4\mathrm{Re}(\delta))e^{-\Gamma_S\tau} + (1 - 4\mathrm{Re}(\delta))e^{-\Gamma_L\tau} + 2(\cos(\Delta m\tau) - 4\mathrm{Im}(\delta)\sin(\Delta m\tau))e^{-\overline{\Gamma}\tau/2}] \\
\overline{\mathcal{P}}_+ &= \mathcal{P}(\overline{K}^0{}_{t=0} \to K^0{}_{t=\tau}) \\
&= \frac{1}{4}[1 + 4\mathrm{Re}(\varepsilon)][e^{-\Gamma_S\tau} + e^{-\Gamma_L\tau} - 2\cos(\Delta m\tau)e^{-\overline{\Gamma}\tau/2}] \\
\mathcal{P}_- &= \mathcal{P}(K^0{}_{t=0} \to \overline{K}^0{}_{t=\tau}) \\
&= \frac{1}{4}[1 - 4\mathrm{Re}(\varepsilon)][e^{-\Gamma_S\tau} + e^{-\Gamma_L\tau} - 2\cos(\Delta m\tau)e^{-\overline{\Gamma}\tau/2}] \\
\overline{\mathcal{P}}_- &= \mathcal{P}(\overline{K}^0{}_{t=0} \to \overline{K}^0{}_{t=\tau}) \\
&= \frac{1}{4}[(1 - 4\mathrm{Re}(\delta))e^{-\Gamma_S\tau} + (1 + 4\mathrm{Re}(\delta))e^{-\Gamma_L\tau} + 2(\cos(\Delta m\tau) + 4\mathrm{Im}(\delta)\sin(\Delta m\tau))e^{-\overline{\Gamma}\tau/2}]
\end{aligned}
$$

where $\Delta m = m_L - m_S$, $\overline{\Gamma} = \Gamma_S + \Gamma_L$, and $m_{S,L}$ and $\Gamma_{S,L}$ denote the $K_{S,L}$ masses and decay widths, respectively. In a measurement, these probabilities translate to different numbers of events recorded, $N_\pm$ and $\overline{N}_\pm$, depending on the detection method for initial and final neutral kaons. The sensitivity to the interference term may be increased and the dependence on the detection efficiencies may be weakened, by considering convenient functions of the measured quantities.

In the measurement reported here, both initial and final neutral kaons are detected by an associated strong interaction (strangeness conserving). The neutral kaons are produced concurrently by antiproton annihilation at rest in a high-pressure, gaseous hydrogen target via the reactions:

$$
\overline{p}p \to \begin{array}{c} K^-\pi^+K^0 \\ K^+\pi^-\overline{K}^0 \end{array}
\tag{1}
$$

each of which has a branching ratio of $\approx 2 \times 10^{-3}$. The conservation of strangeness in the strong interaction dictates that a $K^0$ is accompanied by a $K^-$, and a $\overline{K}^0$ by a $K^+$. Hence, the strangeness of the neutral kaon at production is tagged by measuring the charge sign of the accompanying charged kaon.

In order to identify the strangeness at a later time $t = \tau$, we took advantage of the carbon absorber, shaped as a segment of a hollow cylinder, which had been added to the CPLEAR detector for the regeneration amplitude measurement [20]. Hence we measured the numbers of $K^0$ and $\overline{K}^0$ interacting with the

absorber's bound nucleons in one of the following reactions:

$$K^0 + p \rightarrow K^+ + n \,, \quad \overline{K}^0 + n \rightarrow K^- + p \,, \quad \overline{K}^0 + n \rightarrow \pi^0 + \Lambda(\rightarrow \pi^- p) \,. \tag{2}$$

In the case of initial $K^0$, we denote by $N_+$ and $N_-$ the numbers of $K^0$ and $\overline{K}^0$ which are measured to interact at time $\tau$ in the absorber, and by $\overline{N}_+$ and $\overline{N}_-$ the corresponding numbers for initial $\overline{K}^0$. These numbers $N_\pm$ and $\overline{N}_\pm$ are converted to the probabilities $\mathcal{P}_\pm$ and $\overline{\mathcal{P}}_\pm$ using the cross sections of the reactions (2) and the detection efficiencies of the relevant particles. However, all cross sections and efficiencies cancel in the ratios $N_+/\overline{N}_+$ and $N_-/\overline{N}_-$, except for the detection/tagging efficiency of $\overline{K}^0$ relative to $K^0$ at the production. The latter is expressed by the ratio $\xi$ between the detection efficiencies of the accompanying charged $K^\pm\pi^\mp$ pair, Eq. (1), $\xi = \epsilon(K^+\pi^-)/\epsilon(K^-\pi^+)$,

$$\frac{N_+}{\overline{N}_+} = \frac{1}{\xi}\frac{\mathcal{P}_+}{\overline{\mathcal{P}}_+}\,, \quad \frac{N_-}{\overline{N}_-} = \frac{1}{\xi}\frac{\mathcal{P}_-}{\overline{\mathcal{P}}_-}\,. \tag{3}$$

However, if we compare the experimental asymmetry $A_{\Delta m}^{\text{exp}}$,

$$A_{\Delta m}^{\text{exp}} = \frac{\dfrac{N_+}{\overline{N}_+} - \dfrac{N_-}{\overline{N}_-}}{\dfrac{N_+}{\overline{N}_+} + \dfrac{N_-}{\overline{N}_-}}\,, \tag{4}$$

with the phenomenological asymmetry $A_{\Delta m}$,

$$A_{\Delta m} = \frac{\dfrac{\mathcal{P}_+}{\overline{\mathcal{P}}_+} - \dfrac{\mathcal{P}_-}{\overline{\mathcal{P}}_-}}{\dfrac{\mathcal{P}_+}{\overline{\mathcal{P}}_+} + \dfrac{\mathcal{P}_-}{\overline{\mathcal{P}}_-}} = \frac{4\cos(\Delta m\tau)(e^{-\Gamma_S\tau} + e^{-\Gamma_L\tau})e^{-\overline{\Gamma}\tau/2}}{[e^{-\Gamma_S\tau} + e^{-\Gamma_L\tau}]^2 + 4e^{-\overline{\Gamma}\tau}[\cos(\Delta m\tau)]^2}\,, \tag{5}$$

the relative efficiency $\xi$ also cancels. Fitting the experimental data with Eq. (5) as a function of $\tau$ will provide a measurement of $\Delta m$ without assumptions on the unknown efficiencies. In Eq. (5) additional terms, quadratic in T- and CPT-violation parameters of the mixing matrix, are neglected as they were shown to be irrelevant in the fit.

## 3    The CPLEAR detector

The measurement was performed at the Low-Energy Antiproton Ring (LEAR) at CERN with the CPLEAR detector [21], shown in Fig. 1. The 200 MeV/$c$ antiprotons were extracted from LEAR with an intensity of $10^6$ particles per second and stopped inside a cylindrical gaseous hydrogen target (27 bar pressure). The target (11 mm radius) was surrounded by a small cylindrical proportional chamber PC0 (15 mm radius, 1 mm pitch, $> 99.5\%$ efficiency). A tracking detector, located inside a solenoid (1 m radius, 3.6 m long) providing a 0.44 T magnetic field parallel to the beam, consisted of two layers of proportional chambers (PC1, PC2), six layers of drift chambers and two layers of streamer tubes. A hodoscope of 32 threshold Cherenkov counters (C) sandwiched between two scintillator hodoscopes (S1, S2) provided charged-particle identification (Cherenkov light, time of flight and energy loss). A thin silicon detector in front of the target entrance window ensured the presence of an incoming antiproton, thus rejecting background events resulting from interactions in the target support structure. The arrangement enabled the measurement of neutral-kaon decay rates in the region of 0 to 20 $\tau_S$, where $\tau_S$ denotes the $K_S$ mean life. Fast and efficient background rejection was achieved on-line by a multilevel trigger system. The data for the present measurement are a subset of the data taken for the regeneration measurement [20]. The latter were taken under the same detector and trigger conditions as for the CP-violation measurement, except for the presence of the absorber. The absorber had an opening angle of $115°$ and a thickness of 2.5 cm, with an inner radius of 5.8 cm and a length of 25.5 cm, and allowed neutral-kaon interactions to be measured within the time interval $1.3 - 5.3\ \tau_S$. About $5.6 \times 10^8$ triggers were recorded.

## 4    Event Selection

The events to be selected are $\overline{p}p$ annihilations into either channels of Eq. (1), at a primary vertex inside the target, followed by the production of a charged-kaon or a $\Lambda$ in one of the reactions of Eq. (2), at a secondary vertex inside the absorber. When a charged kaon is produced (first two channels of Eq. (2), the events contain a total of three charged tracks (the proton being too slow to be detected). The $\Lambda$ events contain instead four charged tracks. Thus, a first selection requires the number of tracks to be equal to three (K events, see Section 4.2) or four ($\Lambda$ events, see Section 4.3), with a total charge of $\pm 1$ (in units of e charge) or zero, respectively. No track should have an unphysical fitted momentum, i.e. less than $60 \text{ MeV}/c$ (below which the track would not reach the inner scintillator S1) or above $1 \text{ GeV}/c$. To allow clean particle identification, no more than one track should enter any S1 sector.

The geometrical cuts are mainly applied on quantities measured in the transverse view of the event, using a $(r, \phi)$ reference frame, with its origin on the solenoidal magnet axis ($z$ axis), see Fig. 1. The successive cuts are outlined below. The cuts on any variable are fixed at $\pm 2\sigma$ from the center of the measured distribution fitted with a Gaussian, see for instance Fig. 2.

### 4.1    Selection of the $\overline{p}p$ annihilation channels

The selection of either reactions (1) requires a track pair from the primary vertex with the following conditions:

– At least one charged-kaon candidate, defined as a track associated to a $S1\overline{C}S2$ signal from the scintillator-Cherenkov-scintillator sandwich, with a momentum component $p_T > 300 \text{ MeV}/c$ in the transverse plane, and an energy loss in the inner scintillator S1 consistent with the particle being a kaon.

– The charged-kaon candidate should be crossing the other track at a vertex inside the target ($r < 1.5$ cm and $-3.5 \text{ cm} < z < 6 \text{ cm}$), and at an angle $\theta < 168°$.

– To eliminate a large number of unwanted, very early decay-time $K_S$ decays as well as background multikaon and multipion annihilations, no more than two hits should be found in PC0, each one being within $\Delta\phi < 0.2$ rad of a primary track.

– Offline, the primary charged kaon and the associated pion are the same tracks as those used online to satisfy the trigger conditions. Moreover, fitting the primary pair kinematics with Eq. (1) results in a 1C-fit probability $> 2.5\%$, and the square of the neutral-kaon mass (calculated as missing mass with the momenta returned by the fit) is within $0.20 \text{ GeV}^2/c^4$ of the central value.

### 4.2    Selection of secondary $K^\pm$ events

These are three-track events where the neutral kaon undergoes a charge exchange in the absorber ($K^0 p \rightarrow K^+ n$ , $\overline{K}^0 n \rightarrow K^- p$). Their signature is the presence, beside the primary $K\pi$ pair, of one charged track (secondary) with the following requirements:

– The track is a $K^\pm$ candidate, with a $S1\overline{C}S2$ signature and an energy loss in S1 within four standard deviations of the average Bethe-Bloch value. From the particle's measured momentum and velocity, the mass $m_{K^\pm}$ is obtained. Only events with values of $m_{K^\pm}^2$ within 0.16 or 0.18 $\text{GeV}^2/c^4$ of the central value are considered, for velocity measurement by energy loss or time of flight, respectively.

– The track originates away from the target, from an interaction inside the absorber. Thus, PC0 has no hits within $\Delta\phi < 0.2$ rad of the track, while PC1 and PC2 have hits within the same distance. The projections of the neutral-kaon path and of the secondary track on the transverse plane form the secondary vertex with coordinates $r$ and $\phi$, $5.3 \text{ cm} < r < 9.2 \text{ cm}$ and $-56° < \phi < +58°$. The angular distance of the two projections at the mean radius of the absorber is $\Delta\phi < 0.18$ rad.

### 4.3    Selection of secondary $\Lambda$ events

These are four-track events where a $\overline{K}^0$ interacts in the absorber as $\overline{K}^0 n \rightarrow \pi^0 \Lambda (\rightarrow \pi^- p)$. Their signature is the presence, beside the primary $K\pi$ pair, of another track pair, with the following requirements:

– The two tracks originate away from the target. Thus PC0 has no hits within $\Delta\phi < 0.2$ rad of each track.

3

- One track is a p candidate, with a positive charge, a S1$\overline{\text{C}}$ signature, and a mass $m_p$ with a squared value (from momentum and time of flight) within $0.38 \text{ GeV}^2/c^4$ of the central value.
- The fit to the two-track invariant mass has a probability $> 5\%$ for the $\Lambda$-mass hypothesis, and $< 15\%$ for the $\text{K}_\text{S}$ $(\to \pi^+\pi^-)$ hypothesis.
- The $\Lambda$ originates from an interaction inside the absorber, that is the projection of the $\Lambda$ path on the transverse plane intersects the $\overline{\text{K}}^0$ path projection at the secondary vertex with coordinates $r$ and $\phi$, $5.3 < r < 9.2$ cm, and $-56° < \phi < +58°$. The angular distance of the $\overline{\text{K}}^0$ and $\Lambda$ projections at the mean radius of the absorber is $\Delta\phi < 0.15$ rad.

## 4.4 Final data samples

After applying the above cuts, $1.1 \times 10^4$ K$^+$ events, $2.0 \times 10^3$ K$^-$ events and $1.3 \times 10^4$ $\Lambda$ events remained. Figure 3, showing the azimuthal distributions of the secondary vertices ($\phi$ cuts released), indicates that the background events are very few, as extrapolated from outside the $\phi$ region covered by the absorber, between $-56°$ and $+58°$. Inside that region, the distributions are not flat, especially in the case of secondary K$^\pm$ events, as a consequence of the trigger operating mode – the trigger searching for a single (primary) K$^\pm$. As the direction of the scanning was unimportant, it was arbitrarily chosen to search first along the positive angles. In the special case of the present analysis where a secondary kaon is looked for, at positive angles, this kaon is encountered first in the trigger search, and the event is rejected in the offline analysis (last requirement in Section 4.1).

Figure 4 shows the radial distributions of the secondary vertices ($r$ cuts released). These were best fitted by a uniform distribution (from 6.25 to 8.30 cm) folded with a Gaussian of $\sigma = 0.50$ cm for K$^\pm$ events, and $\sigma = 0.65$ cm for $\Lambda$ events, respectively. The quality of our measurements was checked by estimating the $\Lambda$ mean lifetime, which was found to be $\tau_\Lambda = (2.60 \pm 0.03_{stat} \pm 0.10_{syst}) \times 10^{-10}$ s, in agreement with the current value $\tau_\Lambda = (2.632 \pm 0.020) \times 10^{-10}$ s [22].

The time of the interaction, $\tau$, is determined from the secondary-vertex position and the neutral-kaon momentum (as given by the 1C fit, Section 4.1). The $N_+(\tau)$ and $\overline{N}_+(\tau)$ distributions are obtained from the sample of secondary K$^+$ events. For $N_-(\tau)$ and $\overline{N}_-(\tau)$ one can use the secondary K$^-$ events alone, the $\Lambda$ events alone, or the sum of the K$^-$ and $\Lambda$ samples. With these distributions, we form asymmetries $A^{\text{exp}}_{\Delta m}(\tau)$, Eq. (4) for each type of $\overline{\text{K}}^0$ tagging in the final state, and also for the complete set of events with a $\overline{\text{K}}^0$ in the final state.

## 5 Fit

Each of the three sets of measured asymmetries $A^{\text{exp}}_{\Delta m}$, formed with the $N_\pm$ and $\overline{N}_\pm$ samples defined above, was fitted with Monte Carlo simulations of the asymmetry $A_{\Delta m}(\tau)$, Eq. (5), performed for values of $\Delta m$ in the range $(0.515 - 0.545) \times 10^{10} \hbar/\text{s}$. The simulations included the neutral-kaon momentum distributions, the $\mathcal{P}_\pm$ and $\overline{\mathcal{P}}_\pm$ probabilities, the secondary-vertex spatial resolutions as well as a time resolution of $0.025\ \tau_\text{S}$ due to the uncertainty on the determination of the K$^0$ momentum; for $\Gamma_{\text{S,L}} = 1/\tau_{\text{S,L}}$ the world-average values [22] ($\tau_\text{S} = (89.35 \pm 0.08) \times 10^{-12}$ s and $\tau_\text{L} = (5.15 \pm 0.04) \times 10^{-8}$ s) were used. The simulated asymmetries were compared to the experimental asymmetries $A^{\text{exp}}_{\Delta m}$, and the values of $\Delta m$ corresponding to the minimum $\chi^2$ were determined. The results are reported in Table 1. Owing to the agreement between the values obtained with the two ways of tagging $\overline{\text{K}}^0$, our final result is that given for the (K$^-$+$\Lambda$) sample, shown in Fig. 5.

| $\overline{\text{K}}^0$ tagging | K$^-$ | $\Lambda$ | K$^-$+$\Lambda$ |
|---|---|---|---|
| $\Delta m$ [$10^{10}\hbar$/s] | $0.5253 \pm 0.0106$ | $0.5357 \pm 0.0066$ | $0.5343 \pm 0.0063$ |
| $\chi^2$/ndf | 31/41 | 57/56 | 53/56 |

Table 1: $\Delta m$ values obtained by the fit.

## 6 Systematic errors

Various sources of systematic uncertainties were investigated :
- the uncertainty on $\Gamma_\text{S}$ (the sensitivity to $\Gamma_\text{L}$ is negligible),
- the dependence of the efficiencies on momentum,

4

- the geometrical parameters included in the Monte Carlo simulation,
- the binning and fit range,
- the choice of cuts for the selection criteria.

These uncertainties are summarized in Table 2

| Source | $\Delta m \, [10^{10}\,\hbar/\text{s}]$ |
|---|---|
| $\Gamma_\text{S}$ | 0.0010 |
| efficiencies | 0.0005 |
| Monte Carlo | 0.0015 |
| binning and fit range | 0.0005 |
| selection criteria | 0.0015 |
| Total | 0.0025 |

Table 2: Evaluation of systematic errors

## 7 Final results and conclusion

Our final result is the following :

$$\Delta m = (0.5343 \pm 0.0063_\text{stat} \pm 0.0025_\text{syst}) \times 10^{10}\,\hbar/\text{s}$$

This result is in good agreement with the current values [22]: $\Delta m = (0.5300 \pm 0.0012) \times 10^{10}\,\hbar/\text{s}$ (fit), or $\Delta m = (0.5307 \pm 0.0015) \times 10^{10}\,\hbar/\text{s}$ (average). Our measurement, though not improving on the current world-average error, has the merit of relying only on strong interactions to tag the kaon strangeness. Moreover, the only parameter of the neutral-kaon system which enters the measurement, apart from $\Delta m$, is the $K_\text{S}$ mean lifetime. We conclude that this measurement provides a valuable input for $\Delta m$ in many CPT tests.

## References

[1] M. Gell-Mann and A. Pais, Phys. Rev. 97 (1955) 1387.

[2] A. Pais and O. Piccioni, Phys. Rev. 100 (1955) 1487.

[3] S.B. Treiman and R.G. Sachs, Phys. Rev. 103 (1956) 1545.

[4] E. Boldts, D.O. Caldwell and Yash Pal, Phys. Rev. Lett. 1 (1958) 150.

[5] W.F. Fry and R.G. Sachs, Phys. Rev. 109 (1958) 2212.

[6] V.L. Fitch, P.A. Piroue, R.B. Perkins, Nuovo Cimento 22 (1961) 1160.

[7] U. Camerini et al., Phys. Rev. 128 (1962) 362.

[8] K.M. Case, Phys. Rev. 103 (1956) 1449.

[9] M.L. Good, Phys. Rev. 106 (1957) 591.

[10] M.L. Good, Phys. Rev. 110 (1958) 550.

[11] F. Muller et al., Phys. Rev. Lett. 4 (1960) 418 ; R.H. Good et al., Phys. Rev. 124 (1961) 1223.

[12] M. Cullen et al., Phys. Lett. B32 (1970) 523.

[13] C. Geweniger et al., Phys. Lett. B52 (1974) 108.

[14] L.K. Gibbons et al., E731, Phys. Rev. Lett. 70 (1993) 1198.

[15] B. Schwingenheuer et al., E773, Phys. Rev. Lett. 74 (1995) 4376.

[16] W.A.W. Melhop et al., Phys. Rev. 172 (1968) 1613.

[17] D.G. Hill et al., Phys. Rev. D4 (1971) 7.

[18] S. Gjesdal et al., Phys. Lett. B52 (1974) 113.

[19] A. Angelopoulos et al., CPLEAR Collaboration, Phys. Lett. B 444 (1998) 38.

[20] A. Angelopoulos et al., CPLEAR Collaboration, Phys. Lett. B 413 (1997) 422.

[21] R. Adler et al., CPLEAR Collaboration, Nucl. Instrum. Methods A 379 (1996) 76.

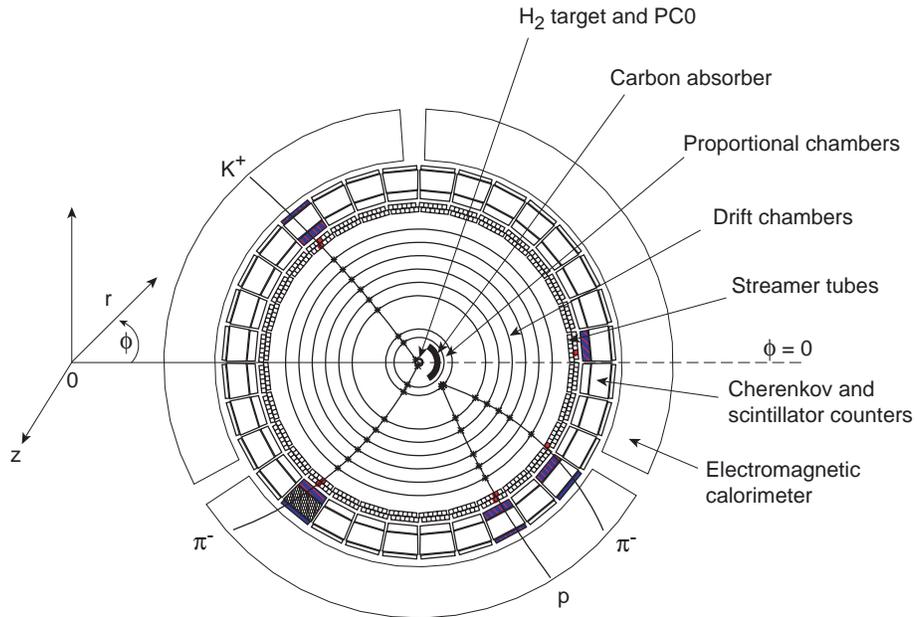[22] D.E. Groom et al., Particle Data Group, Eur. Phys. J. C15 (2000) 1.

Figure 1: Transverse view of the detector at the centre of the experiment (the $z$ axis coincides with the solenoidal magnet axis), and display of an event. The display shows, as a result of a $\overline{p}p$ annihilation, the $K^+\pi^-$ pair produced together with a $\overline{K}^0$. The latter, by interacting in the carbon absorber, produces a $\Lambda$ subsequently decaying to $p\pi^-$ (also shown).
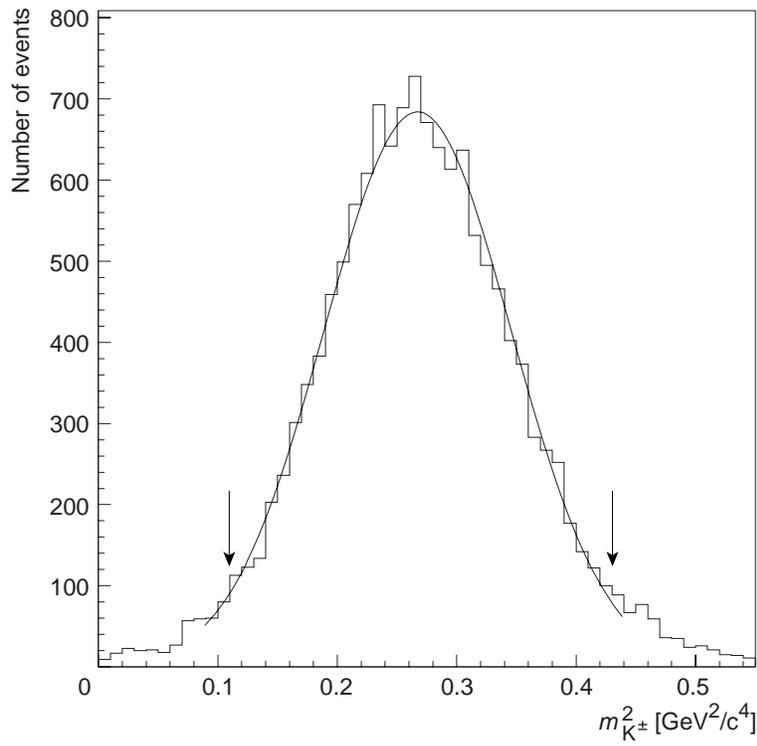
Figure 2: $m^2_{K^\pm}$ distribution; $m_{K^\pm}$ is the measured mass of a secondary charged kaon. The arrows correspond to the cuts (see text).
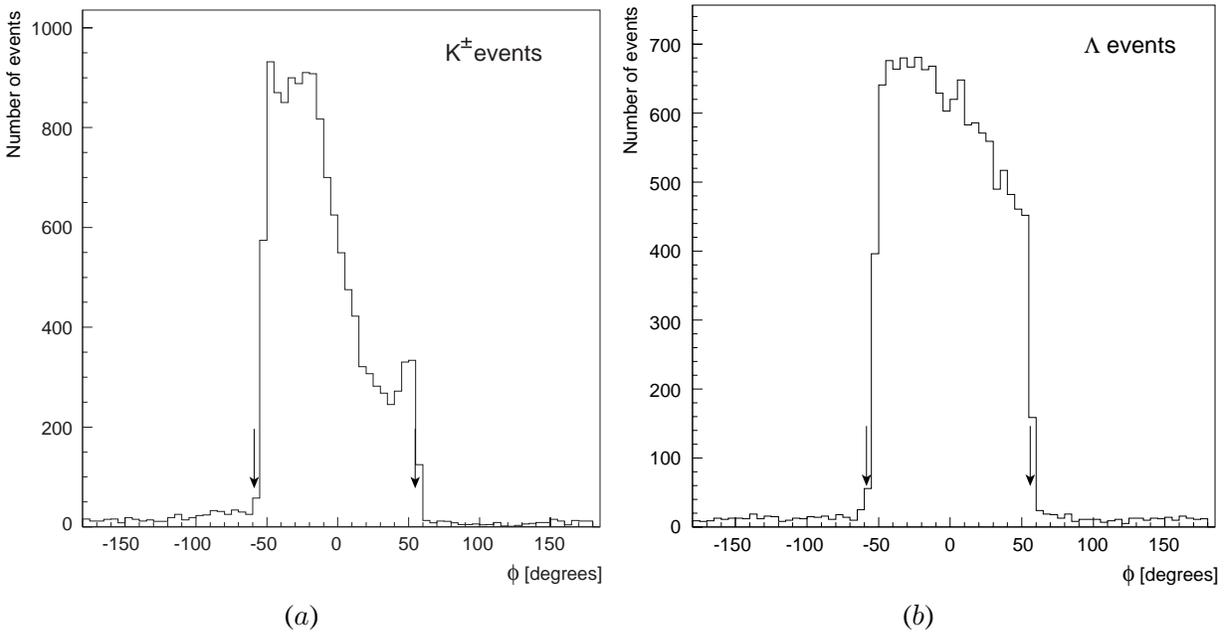


Figure 3: Azimuthal ($\phi$) distribution of the secondary vertices after all selections ($a$) for $K^\pm$ events; ($b$) for $\Lambda$ events. The events are well localized in the interval $[-56°, +58°]$ corresponding to the position of the absorber. Outside this interval the background is very small; the arrows indicate the cuts. The large asymmetry between the number of events recorded for negative and positive angles is related to the trigger operating mode (see text).
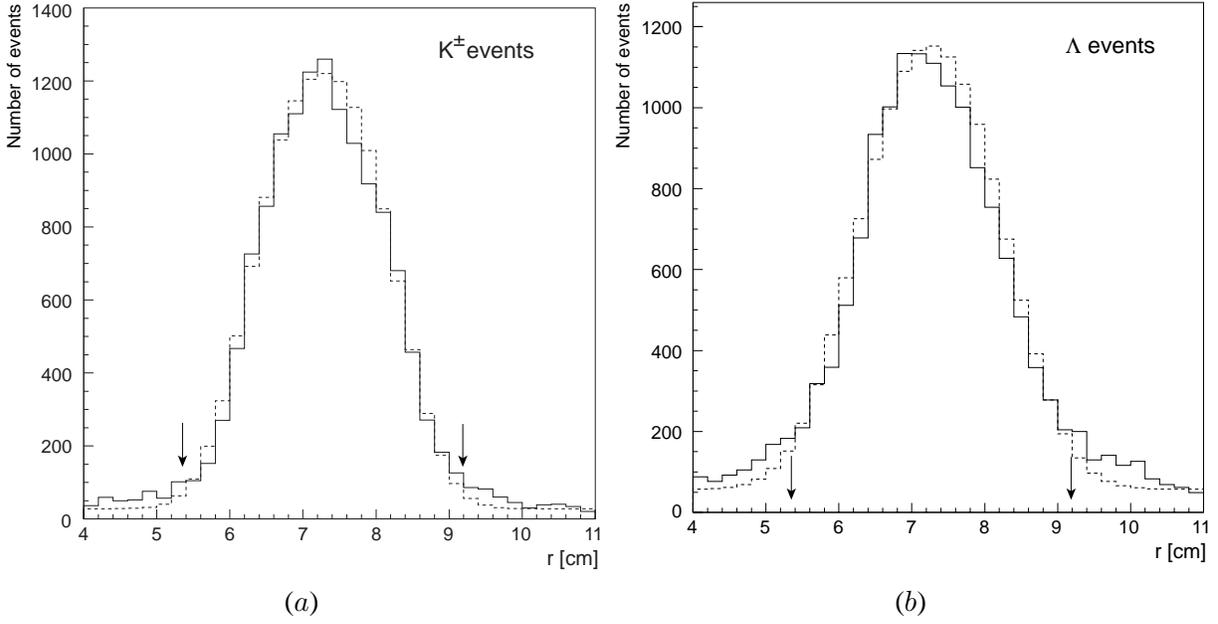
7

(a)    (b)

Figure 4: Radial distributions of the secondary vertices (a) for the $K^{\pm}$ events and (b) for the $\Lambda$ events. The measured distributions (solid lines) are compared with the simulated distributions (dashed lines), see text. The arrows indicate the cuts.
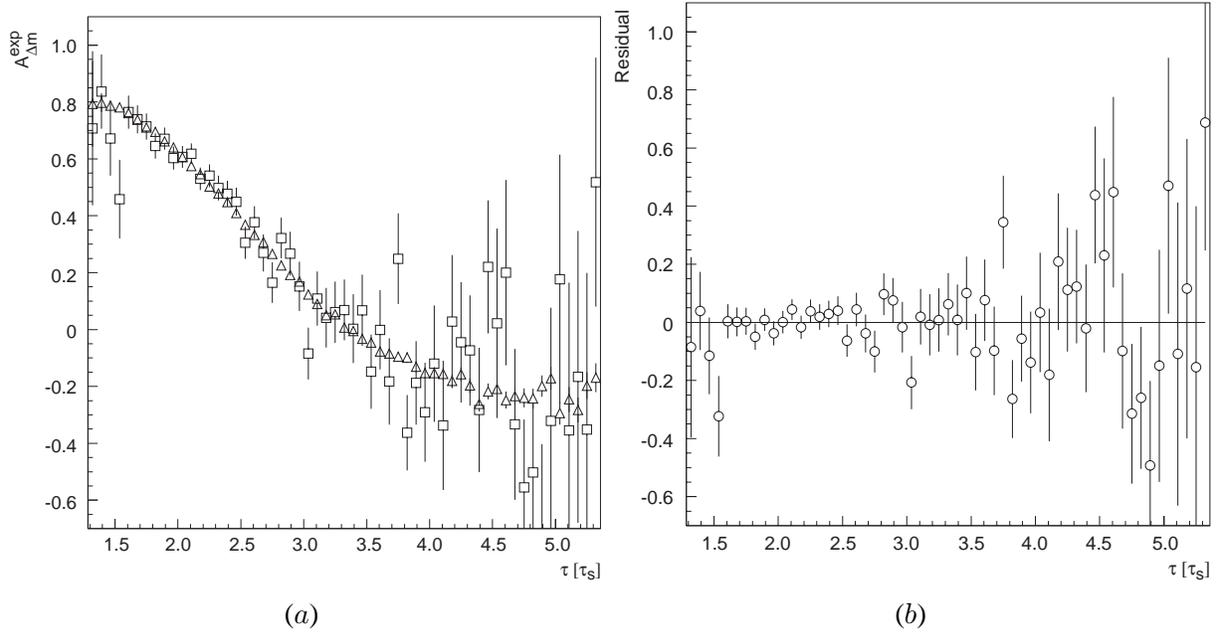


(a)    (b)

Figure 5: (a) Best fit to the data points $A_{\Delta m}^{exp}(\tau)$(squares) with the simulated asymmetries (triangles) for the $(K^- + \Lambda)$ sample, see text. (b) Distribution of the fit residuals.